

# Carbon-based ultrabroadband tunable terahertz metasurface absorber

Aiqiang Nie<sup>1</sup>, Xiaoyong He<sup>1,2,\*</sup> and Wenhan Cao<sup>1,2,3,\*</sup>

<sup>1</sup>ShanghaiTech University, School of Information Science and Technology, Shanghai, China

<sup>2</sup>Shanghai Normal University, Mathematics and Science College, Department of Physics, Shanghai, China

<sup>3</sup>Shanghai Engineering Research Center of Energy Efficient and Custom AI IC, Shanghai, China

**Abstract.** Carbon-based materials, such as graphene and carbon nanotubes, have emerged as a transformative class of building blocks for state-of-the-art metamaterial devices due to their excellent flexibility, light weight, and tunability. In this work, a tunable carbon-based metal-free terahertz (THz) metasurface with ultrabroadband absorption is proposed, composed of alternating graphite and graphene patterns, where the Fermi level of graphene is adjusted by varying the applied voltage bias to achieve the tunable ultrabroadband absorption characteristics. In particular, when the Fermi level of graphene is 1 eV, the absorption coefficient exceeds 90% from 7.24 through 16.23 THz, and importantly, the absorption bandwidth reaches as much as 8.99 THz. In addition, it is polarization-insensitive to incident waves and maintains a high absorption rate at an incident angle of up to 50 deg. This carbon-based device enjoys higher absorption bandwidth, rates, and performance compared to conventional absorbers in the THz regime and can be potentially applied in various fields, including THz wave sensing, modulation, as well as wearable health care devices, and biomedicine detection.

Keywords: terahertz; metamaterial; metasurface; absorber; graphene; graphite; carbon.

Received Oct. 30, 2023; revised manuscript received Nov. 29, 2023; accepted for publication Dec. 11, 2023; published online Jan. 10, 2024.

© The Authors. Published by SPIE and CLP under a Creative Commons Attribution 4.0 International License. Distribution or reproduction of this work in whole or in part requires full attribution of the original publication, including its DOI.

[DOI: [10.1117/1.APN.3.1.016007](https://doi.org/10.1117/1.APN.3.1.016007)]

## 1 Introduction

Terahertz (THz) wave is electromagnetic radiation with a frequency range typically spanning from 0.1 to 10 THz, which has great application prospects in the fields of communication, sensing, spectroscopy, and imaging.<sup>1-4</sup> However, the lack of high-performance functional devices still remains one of the most important factors hindering the development of THz technology.<sup>5,6</sup> Interestingly, in the past few decades, the modern integrated circuit (IC) industry and microelectromechanical systems fabrication techniques involving photolithography have made possible the fabrication of microstructures with length scales that happen to fall within the range of THz wavelength. Thus, artificially structured elements arranged in a periodic manner, namely metamaterials or metasurfaces, which can achieve unusual and favorable electromagnetic responses and

characteristics have been studied intensively in the past few decades.<sup>7,8</sup> The excellent properties of metamaterials can greatly promote the application of THz technology,<sup>9</sup> such as filters,<sup>10</sup> absorbers,<sup>11</sup> and polarization converters.<sup>12</sup> Among these various metamaterial devices, absorbers play an important role in that their perfect characteristics can be further applied in many fields including electromagnetic stealth<sup>13</sup> and optical filters.<sup>14</sup> The concept of a metamaterial absorber was first proposed by Landy et al. in 2008, where the split-ring resonator, dielectric layer, and metal wire resonators were used to achieve perfect microwave absorption.<sup>15</sup> Subsequently, various structures of metamaterial absorbers were proposed, and the operation bandwidth gradually expanded from radio frequencies to other spectral ranges.<sup>16</sup>

However, as is also one of the major drawbacks of IC industry from a manufacturing perspective, once the structural pattern of the absorbers is determined and fabricated, their electromagnetic performances become fixed and stay invariant to external conditions. Therefore, tunable THz absorbers using various mechanisms at this stage are highly demanded for their enormous potential and advantages.<sup>17</sup>

\*Address all correspondence to Xiaoyong He, [xyhethz@hotmail.com](mailto:xyhethz@hotmail.com); Wenhan Cao, [whcao@shanghaitech.edu.cn](mailto:whcao@shanghaitech.edu.cn)

Nowadays, researchers have proposed some dynamically tunable metamaterial absorbers.<sup>18–20</sup> The tunable materials mainly include novel 2D materials, such as graphene,<sup>21–23</sup> molybdenum disulfide (MoS<sub>2</sub>), and phase change materials, such as vanadium oxide (VO<sub>2</sub>).<sup>24–26</sup> Also, most common metamaterial absorbers involve metal parts, but the change of electrical performance of the metal at higher frequencies would lead to the performance degradation of the device.<sup>27,28</sup> In THz surface plasmonic and metamaterial applications, metal thin films can seriously scatter due to defects, grain boundaries, and other reasons, resulting in lower conductivity than carbon materials.<sup>29</sup> At this point, carbon-based materials provide a good alternative to solve those problems. For instance, graphene is a material composed of single-layer carbon atoms, which has unique and excellent properties, such as high carrier mobility, high Fermi velocity, and good mode confinement.<sup>30–32</sup> Furthermore, its electrochemical potential can be adjusted through electrostatic gating, magnetic field, or optical excitations.<sup>33</sup> Graphite also would be an excellent THz absorber with good shielding effectiveness, small reflection, and better temperature stability.<sup>34,35</sup> In recent years, absorber structures based on graphite resonators have been reported to achieve broadband THz absorption, but they cannot be dynamically tuned.<sup>36–38</sup>

So far, some multilayer graphene-based structures,<sup>39</sup> multilayer VO<sub>2</sub>-based structures,<sup>40</sup> or multilayer metal/dielectric structures<sup>41</sup> have been designed to achieve tunable ultra-wideband absorption bandwidth. However, these structures greatly increase the difficulty of manufacturing, and the performance of devices is not reliable due to the characteristics of metals in certain environments. To overcome these research challenges, in this work, we designed a carbon-based metasurface absorber and studied it through a series of numerical analyses. The proposed absorber utilizes the graphite and graphene material as resonator, and graphite material as the back reflecting layer, which can provide a wide absorption spectrum in ultra-thin geometric shapes. By adjusting the Fermi level, the width of the bandwidth can be altered. When the Fermi level is 1 eV, the proposed absorber provides absorption of more than 90% in the 7.24 – 16.23 THz frequency range. The bandwidth reaches a maximum of 8.99 THz. Moreover, due to the symmetry of the geometric structure, the absorption characteristics of the absorber are insensitive to the polarization state and incident angle of electromagnetic waves.

## 2 Materials and Methods

The unit cell in this THz metasurface absorber is strategically designed to optimize absorption efficiency mainly based on four factors: geometry, material properties, polarization sensitivity, and tuning mechanisms. Geometrically, the metasurface absorber consists of three layers: a patterned conductive layer composed of periodically arranged concentric ring patterns defining the electromagnetic parameters, a dielectric layer that dissipates electromagnetic waves, and a third absorption layer preventing electromagnetic waves from transmitting to achieve maximum absorption efficiency. From a material perspective, the carbon-based materials help the unit cell to further enhance absorption in the THz regime. The unit cell is structured using a highly symmetric concentric pattern, such that the unit cell exhibits polarization insensitivity with optimized THz absorption. A voltage-controlled tuning mechanism by varying Fermi energy level allows adaptability to different THz frequencies or operational conditions. Collectively, these factors define the

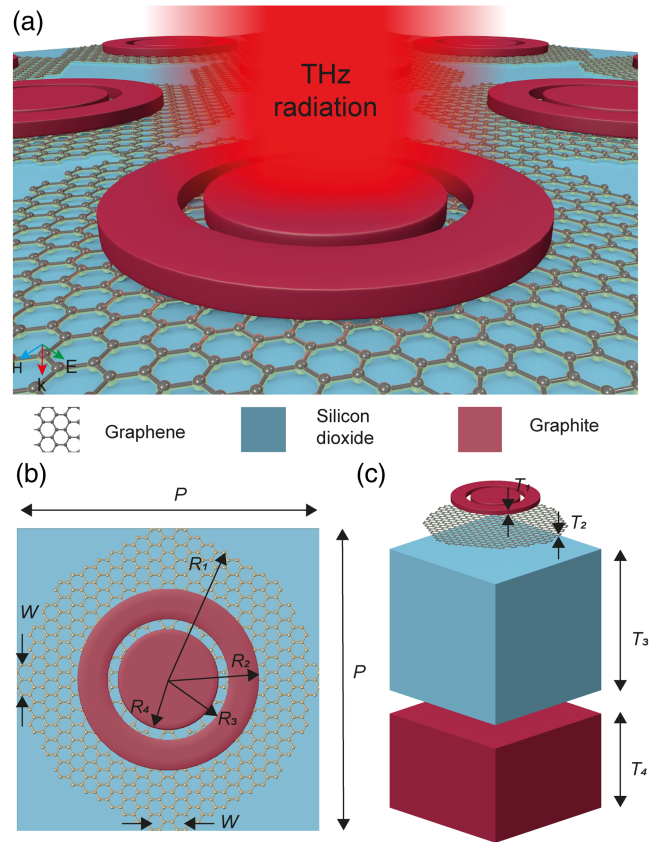


**Fig. 1** Schematic diagram of broadband absorber structure: (a) three-dimensional structure, (b) top view of a unit cell, and (c) split diagram of a unit cell.

design principle and enable our THz metasurface absorber to achieve its intended functionality effectively. Figure 1 presents the geometry of the proposed absorber, and Table 1 shows the corresponding structural parameters. Figure 1(a) is a three-dimensional structure, Fig. 1(b) is the top view of a unit cell, and Fig. 1(c) is the split diagram of a unit cell. The designed absorber unit cell with periodicity  $P$  has a four-layer structure.

**Table 1** Parameters of the designed carbon-based metasurface absorber.

Parameter	Value ( $\mu\text{m}$ )
Unit cell periodicity ( $P$ )	3
Width of graphene interconnects ( $W$ )	0.05
Radius of graphene structure ( $R_1$ )	1.4
Outer radius of graphite ring ( $R_2$ )	0.9
Inner radius of graphite ring ( $R_3$ )	0.6
Radius of graphite circle ( $R_4$ )	0.5
Thickness of graphite ( $T_1$ )	0.1
Thickness of graphene ( $T_2$ )	0.001
Thickness of dielectric layer ( $T_3$ )	3
Thickness of substrate ( $T_4$ )	2

Due to the complete symmetry of the circle, we have designed the upper resonant unit using a circular shape, which is insensitive to electromagnetic wave polarization, making the absorber versatile in accommodating various polarizations of incoming THz radiation. Also, the absence of sharp corners or edges in the circular shape minimizes unwanted scattering and diffraction effects. Furthermore, this reduction in edge effects helps maintain the integrity of the absorbed THz energy within the absorber, thereby improving the overall absorption efficiency. Additionally, circular geometries can be easily scaled for different applications and frequencies, enhancing the practicality and versatility of the metasurface absorber. The top layer is made of graphite material consisting of a circle and a ring. In order to achieve a wider band and realize the tunable function, the lower layer is a circular-shaped graphene layer, and four graphene wires relate to other units to achieve the overall adjustment of the chemical potential energy of graphene when the voltage is applied. The dielectric layer in the middle is silicon dioxide ( $\epsilon_s = 3.9$ ), and the substrate layer is graphite as the back reflecting plane.

The electrical conductivity of graphite can be described by the Drude model

$$\sigma(\omega) = \frac{\epsilon_0 \omega_p^2 \tau}{1 + j\omega\tau}, \quad (1)$$

where  $\epsilon_0$  is the dielectric permittivity of vacuum,  $\omega_p$  is the plasma frequency, and  $\tau$  is the relaxation time of approximately within  $0.1 \times 10^{-13} - 3 \times 10^{-13}$  s.<sup>42</sup> Graphite permittivity  $\epsilon_r$  can be defined from Ampère–Maxwell law given as

$$\epsilon_r(\omega) = \epsilon_{r,\infty}(\omega) + \frac{\sigma(\omega)}{\omega\epsilon_0}, \quad (2)$$

where  $\epsilon_{r,\infty}(\omega)$  is the background dielectric permittivity.<sup>42</sup>

The conductivity of graphene will change due to the influence of Fermi level, relaxation time, angular frequency of incident wave, and ambient temperature. Graphene's conductivity is described by inter-band and intra-band contributions<sup>33,43</sup> as

$$\sigma_g(\omega) = \sigma_1^{\text{intra}}(\omega) + \sigma_2^{\text{inter}}(\omega), \quad (3)$$

$$\sigma_1^{\text{intra}} = \frac{2k_B T e^2}{\pi \hbar^2} \ln \left( 2 \cos h \frac{E_f}{2k_B T} \right) \frac{i}{\omega + i\tau^{-1}}, \quad (4)$$

$$\sigma_2^{\text{inter}} = \frac{e^2}{4\hbar} \left[ H \left( \frac{\omega}{2} \right) + i \frac{4\omega}{\pi} \int_0^\infty \frac{H(\xi) - H(\frac{\omega}{2})}{\omega^2 - 4\xi^2} d\xi \right], \quad (5)$$

$$H(\xi) = \frac{\sinh \left( \frac{\hbar \xi}{k_B T} \right)}{\left[ \cosh \left( \frac{\hbar \xi}{k_B T} \right) + \cosh \left( \frac{E_f}{k_B T} \right) \right]}, \quad (6)$$

where  $\hbar = h/2\pi$  is the reduced Planck constant  $h = 6.62 \times 10^{-34}$  J · s,  $k_B = 1.38 \times 10^{-23}$  J/K is the Boltzman constant,  $e = 1.6 \times 10^{-19}$  C is the electron charge,  $T = 300$  K is the temperature,  $E_f$  is the electrochemical potential or Fermi energy,  $\omega$  is the frequency of incident electromagnetic wave, and  $\tau = 10^{-13}$  s is the relaxation time.

In the THz regime, where the photon energy  $\hbar\omega \ll E_f$ , the inter-band part conductivity is negligible compared to the intra-band. Therefore, the conductivity model of graphene can be expressed by the Drude model

$$\sigma_g(\omega) \approx \frac{e^2 E_f}{\pi \hbar^2} \frac{i}{\omega + i\tau^{-1}}. \quad (7)$$

The Fermi level of graphene can be changed by applying a bias voltage, thereby regulating its surface conductivity. The relationship between the Fermi level of graphene and the bias voltage  $V_{\text{bias}}$  is<sup>44</sup>

$$E_f \approx \hbar v_f \sqrt{\frac{\pi \epsilon_r \epsilon_0 V_{\text{bias}}}{e t_s}}, \quad (8)$$

where  $v_f \approx 1.1 \times 10^6$  m/s is the Fermi level velocity,  $e$  is the electron charge,  $\epsilon_r$  is the dielectric permittivity constant,  $\epsilon_0$  is the dielectric permittivity of vacuum, and  $t_s$  is the dielectric thickness.

The absorption coefficient of the absorber is calculated from  $S$  parameters using

$$A(\omega) = 1 - R(\omega) - T(\omega), \quad (9)$$

where  $R(\omega) = |S_{11}(\omega)|^2$  is the reflectance and  $T(\omega) = |S_{21}(\omega)|^2$  is the transmittance. The thickness of the graphite layer on the substrate is  $2 \mu\text{m}$ , much larger than the skin depth, so the transmittance can be regarded as 0.

## 3 Results

### 3.1 Absorber Evolution

The proposed absorber is realized using the superposition optimization of four different patterns of graphite and patterned graphene, which shows the change of absorbance with frequency when the Fermi level of graphene is 1 eV under different structures, as shown in Fig. 2. The key features of the proposed carbon-based absorber structure are analyzed with Computer Simulation Technology (CST) Microwave Studio (see [Supplementary Material](#) for more details). Fig. S1 shows the simulated structure of the absorber. When there is only a silicon dioxide medium and graphite reflection layer, the

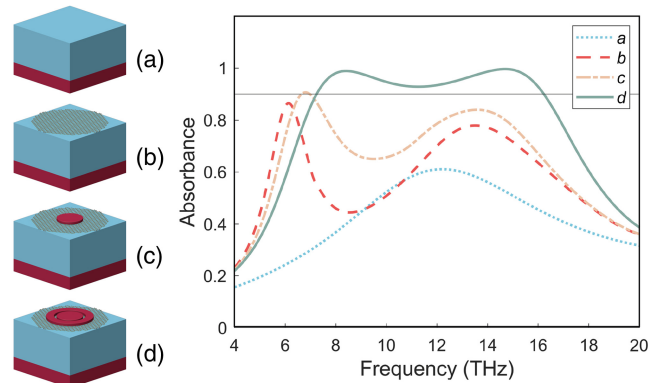


**Fig. 2** (a)–(d) Absorption curves of evolutionary structures ( $E_f = 1$  eV).

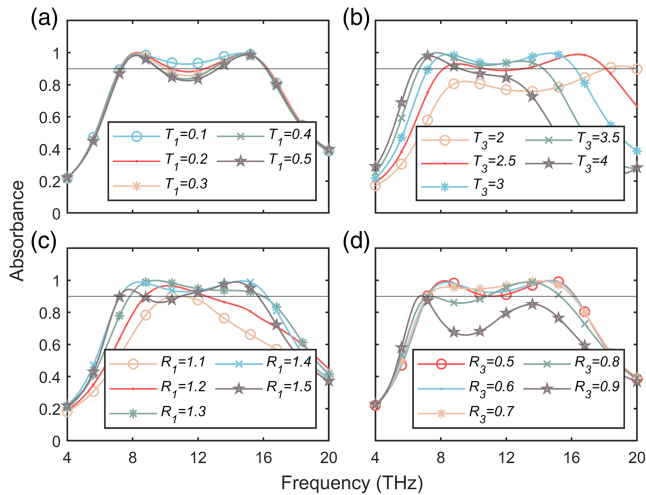


**Fig. 3** (a)–(d) Influence of different structural parameters on the performance of the absorber ( $E_f = 1$  eV).

highest absorption peak of the absorber only reaches about 60%. If a patterned graphene layer is added above, there will be two absorption peaks at 8.35 and 14.70 THz, respectively. The absorption peak is about 85%, and the absorption bandwidth is very narrow. Later, when a small circular graphite layer was added to the graphene layer, the absorption peak further increased to about 90%. Afterwards, a circular ring was added to further increase the absorption peak and bandwidth, reaching a peak of 100% and an absorption bandwidth of 8.99 THz. At this point, the surface plasmon resonance of graphite and graphene is coupled with each other, thereby expanding the absorption bandwidth.

Figure 3 shows the influences of the geometric parameters of the carbon-based metasurface absorber on the resonance frequency and absorption, and the Fermi level is 1 eV. Figure 3(a) shows the effects of the thickness of the top graphite layer mainly affects the absorption of intermediate frequencies. As the thickness of the top graphite layer increases, the absorption intensity of the intermediate frequency will decrease. As shown in Fig. 3(b), when the thickness of the silica material increases from 2 to 4  $\mu\text{m}$ , it has a significant impact on the absorption amplitude and working bandwidth. As the thickness of silicon dioxide gradually increases, the absorption bandwidth gradually decreases and the overall redshift occurs. When the thickness of silica is 3  $\mu\text{m}$ , the absorption strength and width reach their maximum. As shown in Fig. 3(c), the radius of circular graphene also has a significant impact on the absorption bandwidth. When the radius  $R_1$  of circular graphene changes from 1.1 to 1.5  $\mu\text{m}$ , the absorption bandwidth will gradually increase to its maximum at 1.4  $\mu\text{m}$ , and then gradually decrease. Figure 3(d) shows the effect of the inner diameter of the outer ring on the absorption strength.

When  $R_3 = 0.5 \mu\text{m}$ , the outer ring and the middle circle merge into one circle. At this point, the two resonance peaks reach their highest, and the absorption intensity in the middle is about 90% lower. When  $R_3$  decreases, the resonance peak on the left begins to redshift and its intensity decreases. The resonance peak on the right also begins to redshift but its intensity remains unchanged, while the absorption intensity in the middle part begins to increase. After  $R_3$  is greater than or equal to 0.8  $\mu\text{m}$ , it has a significant impact on absorption. When  $R_3 = 0.9 \mu\text{m}$ , the outer circle is gone, only the inner circle.

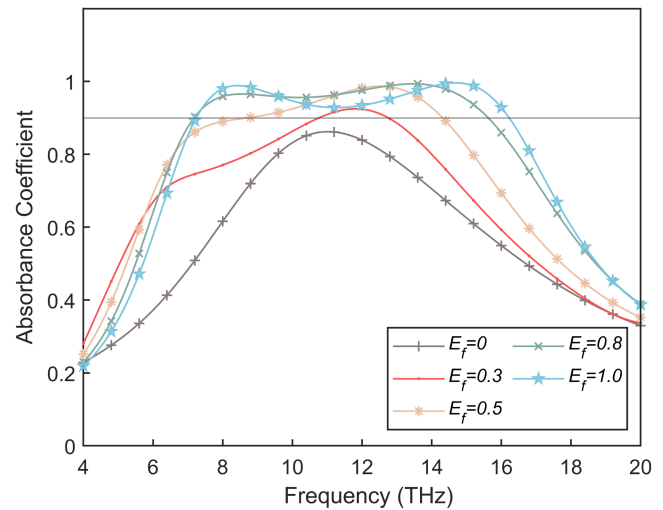


**Fig. 4** Absorption curves of the absorber at 0–1 eV graphene Fermi energy levels (the absorption bandwidth at 1 eV is 8.99 THz).

### 3.2 Fermi Level Change

The absorption spectra of the carbon-based metasurface absorber at different Fermi energy levels are shown in Fig. 4. The change of graphene Fermi level affects the surface conductivity significantly, which destroys the impedance matching between the absorber and the free space impedance, resulting in different absorption spectra. For example, when the Fermi level of graphene increases from 0 to 1 eV, the corresponding absorption band gradually widens, the absorption peak indicates gradual blue shifts and the absorption intensity is also gradually increasing. When the Fermi level increases from 0.3 to 1 eV, the absorption bandwidth has been broadened from 2 THz (10.76 to 12.76 THz) to 8.99 THz (7.24 to 16.23 THz) and the absorption is above 0.9. As the Fermi level increases, the carrier concentration and graphene permittivity increase, and the graphene ribbons manifest better plasmonic properties and interact with THz strongly, resulting in a wider bandwidth. However, when the graphene Fermi level is 0 eV, it behaves just like a thin dielectric layer and cannot absorb THz waves effectively. In this case, the absorption of the metasurface devices mainly results from the graphite layer, on the condition that the absorption rate of THz is  $> 0.8$ , the bandwidth is about 2 THz, i.e., in the range of 10.10–12.68 THz, mainly due to the absorption of THz waves by the graphite structure. When the Fermi energy level is 1 eV, the Fermi energy level reaches the maximum width of 8.99 THz.

### 3.3 Equivalent Medium Theory

Since the geometric size of the periodic unit cell of the metasurface device is far smaller than the wavelength of incident wave, when analyzing the electromagnetic characteristics, it can be regarded as a whole structure, neglecting the interaction of different parts inside the structure. Furthermore, because the structure is basically symmetrical, it can be equivalent to a uniform dielectric plate.<sup>45</sup> The relative impedance, equivalent refractive index, equivalent permittivity, and equivalent permeability of metasurface can be obtained by the S parameter inversion method.<sup>46</sup> The expression is given as

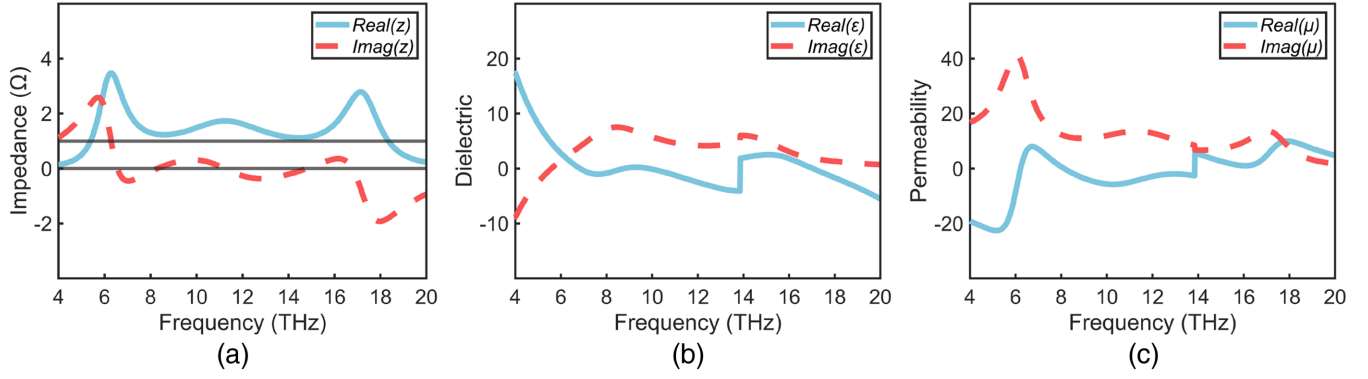


**Fig. 5** Equivalent parameters ( $E_f = 1$  eV): (a) relative impedance, (b) equivalent dielectric constant, and (c) equivalent magnetic permeability.

$$Z = \sqrt{\frac{\mu_{\text{eff}}}{\epsilon_{\text{eff}}}} = \sqrt{\frac{(1 + S_{11})^2 - S_{21}^2}{(1 - S_{11})^2 - S_{21}^2}}, \quad (10)$$

$$n = \frac{1}{kd} \cos^{-1} \left[ \frac{1}{2S_{21}} (1 - S_{11}^2 + S_{21}^2) \right], \quad (11)$$

$$\epsilon_{\text{eff}} = \frac{n}{Z}, \quad (12)$$

$$\mu_{\text{eff}} = nZ. \quad (13)$$

As shown in Fig. 5(a), the real part of the relative impedance approaches 1 and the imaginary part approaches zero in the frequency range of 7.24–16.23 THz. This means that the impedance of the absorber matches that of the free space, where the absorption rate is close to 1 and the reflectivity is close to 0. At this point, as shown in Figs. 5(b) and 5(c), the relative dielectric constant and relative magnetic permeability of the material are equal.

### 3.4 Electrical Circuit Model

The designed ultra-wideband absorber can be verified the response obtained through full-wave simulation by designing an equivalent circuit. The transmission line method is used to design ECM, as shown in Fig. 6(a). The silicon dioxide dielectric

on the graphite can offer impedance  $Z_d$ . The graphite plane at the bottom acts as the reflector and a part of power is absorbed. Its impedance can be considered as  $Z_g$ . The impedance provided by silicon dioxide and graphite plane can be calculated as

$$Z_l = Z_d \left[ \frac{Z_g - jZ_d \tan(k_z T_1)}{Z_d - jZ_g \tan(k_z T_1)} \right], \quad (14)$$

where  $Z_g = \frac{Z_0}{\sqrt{\epsilon_g}}$ ,  $Z_d = \frac{Z_0}{\sqrt{\epsilon_d}}$ , and  $Z_0$  is the free space impedance.  $\epsilon_g$  and  $\epsilon_d$  are the dielectric constants of graphite and silicon dioxide, respectively.

The top plane of graphite is modelled as a series RLC circuit which also can offer the impedance  $Z_1$ . The patterned graphene plane can be modelled as a series LC circuit which offers the impedance  $Z_2$ . Their impedance is computed as  $Z_c = Z_1 || Z_2$ .

The impedance at the input port can be calculated as

$$Z_{\text{in}} = Z_c || Z_l. \quad (15)$$

Finally, the reflection coefficient can be calculated as

$$\Gamma = \frac{Z_{\text{in}} - Z_0}{Z_{\text{in}} + Z_0}. \quad (16)$$

As shown in Fig. 6, the absorption coefficient curve obtained using an equivalent circuit model and full-wave simulation is in good agreement. The parametric settings of the electrical circuit can be found in Fig. S2 in the [Supplementary Material](#).

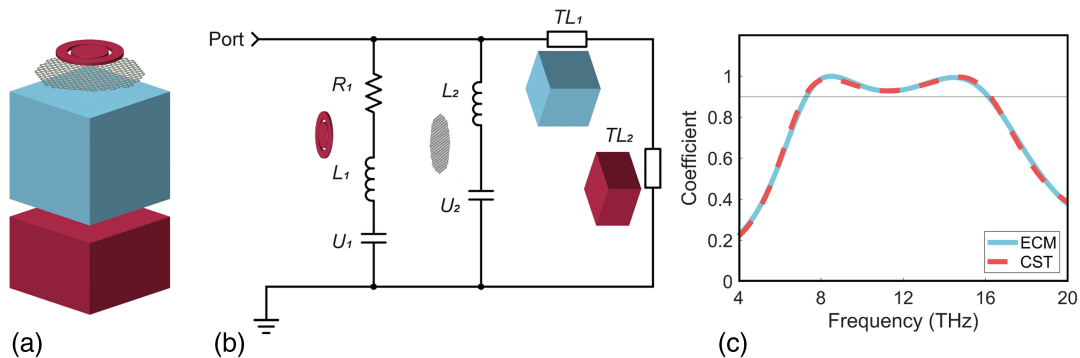


**Fig. 6** (a) split diagram of a unit cell, (b) electrical circuit, and (c) comparison of absorption curves obtained by simulation and ECM ( $E_f = 1$  eV).

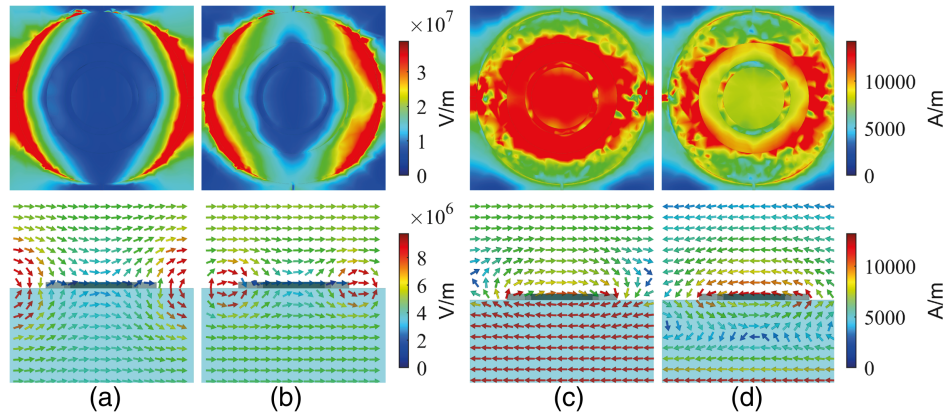


**Fig. 7** The absolute field distribution and field distribution of vector ( $E_f = 1$  eV): (a) E-field ( $f = 8.34$  THz), (b) E-field ( $f = 14.66$  THz), (c) H-field ( $f = 8.34$  THz), and (d) H-field ( $f = 14.66$  THz).

### 3.5 Resonant Mode Analysis

To explain the mechanism of the absorber, the energy distribution of two resonance frequencies, 8.34 and 14.66 THz, are selected at a Fermi level of 1 eV. Their electromagnetic distribution, current density distribution, power loss, and incident angle are discussed, respectively.

The first row of Fig. 7 shows the distribution of the absolute field, and the second row shows the vector distribution of the field. The electric field is mainly distributed on both sides of the circular graphene layer at 8.34 THz, and the magnetic field is mainly distributed on the graphite ring. When the frequency continues to increase to 14.66 THz, the electric field on the circular graphene layer begins to strengthen, and the magnetic field distribution is mainly around the graphite. The field distribution at 8.34 and 14.66 THz corresponds to the fundamental and higher-order magnetic dipoles.

The power loss density and current distribution on the proposed carbon-based absorber are shown in Fig. 8. At the frequency of 8.34 THz, the power loss in the absorber mainly occurs in the patterned graphene layer, while the power loss in the circular graphite structure mentioned above is relatively low. At the frequency of 14.66 THz, there is no significant

change in the distribution of power loss. It can be seen that patterned graphene absorbs most of the energy, while the presence of a circular graphite layer further enhances energy absorption. When the resonance frequency is 8.34 THz, the current direction in the top graphene layer is consistent with the current direction in the bottom graphite. Furthermore, the surface plasmon resonance is excited between the interface of the graphene and the dielectric layer silicon dioxide, enhancing the absorption performance of the absorber. When the resonance frequency reaches 14.66 THz, the current on the surface of the top resonator is concentrated and distributed on the patterned graphene layer. The current generates electric dipole resonance from right to left, while the current direction of the graphite reflecting layer is opposite to the current direction of the top graphene and forms a circuit, which excites and forms magnetic dipole resonance.

In the practical application of devices, external incident THz waves may come back from different directions, so it is necessary to study the sensitivity of devices to polarization angles. Figures 9(a) and 9(b) show the absorption spectra of the device in transverse electric (TE) and transverse magnetic (TM) mode as a function of the incident angle, respectively. For TE mode, the low resonance frequency remains stable at a span of 50 deg, while the high resonance exhibits a slight increase in blue shift

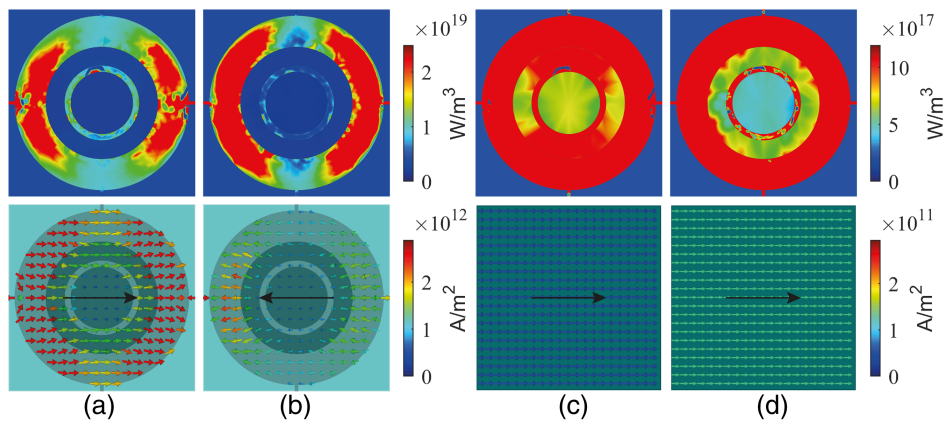


**Fig. 8** The power loss (first row) on graphene (left) and graphite (right) and current density (second row) on the top (left) and bottom surfaces (right) in the absorber at frequency ( $E_f = 1$  eV): (a) and (c) 8.34 THz; (b) and (d) 14.66 THz.

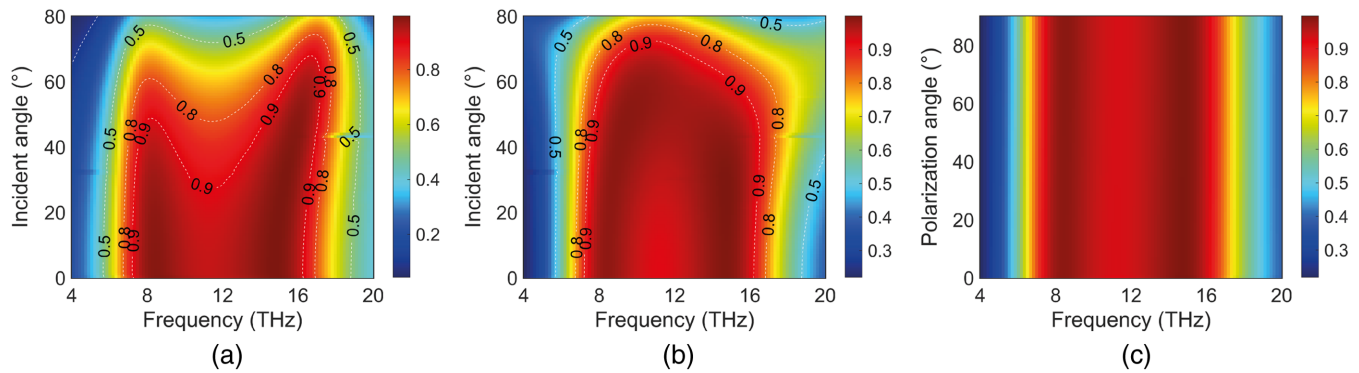


**Fig. 9** The absorption spectrum of the absorber ( $E_f = 1$  eV): (a) different incident angles of TE mode, (b) different incident angles of TM mode, and (c) different polarization angles.

**Table 2** Comparison of performance parameters with those of other absorbers.

Reference	Material	Frequency range (THz) ( $A > 90\%$ )	Bandwidth (THz)	Thickness ( $\mu\text{m}$ )	Insensitive to $\Phi$	Tunable
18	VO <sub>2</sub> /metal	2.6 to 7.5	4.9	76.5	Yes	Yes
21	Metal/graphene	3.4 to 9.1	5.7	9.5	Yes	Yes
47	VO <sub>2</sub> /metal	1.85 to 4.3	2.45	12.4	Yes	Yes
36	Graphite	0.65 to 3.03	2.38	50.2	Yes	No
37	Graphite	6.26 to 13.05	6.79	7	Yes	No
48	Graphene/metal	3.69 to 9.77	6.08	7.101	Yes	Yes
49	Graphene/metal	7 to 9.25	2.25	5.101	Yes	Yes
This work	Graphene/graphite	7.24 to 16.23	8.99	5.101	Yes	Yes

bandwidth. The absorption coefficient does not change significantly by more than 90% within the range of 0–30 deg, but gradually decreases from 30 to 60 deg. After 60 deg, there is a significant decrease in the absorption coefficient. At 0–30 deg, there is no significant change in the absorption bandwidth, but after 30 deg, the bandwidth splits into two. For TM mode, the absorption coefficient does not change significantly by more than 90% within the range of 0–55 deg, but gradually decreases from 55 to 70 deg, and there is a significant decrease in absorption coefficient after 70 deg. The bandwidth remains basically unchanged from 0 to 50 deg and gradually narrows after 50 deg. Figure 9(c) shows the absorption intensity of the absorber at different polarization angles from 0 to 90 deg, indicating that the absorption intensity remains basically unchanged, indicating that the device is insensitive to polarization angles due to the symmetry of the design.

As shown in Table 2, some key parameters of the proposed carbon-based absorber were compared with other absorbers. It can be seen that the proposed absorber provides an ultra-thin and simple metal-free structure, with a wider absorption bandwidth and tunable bandwidth at a thinner thickness, greatly improving the applicability of the absorber. This is an advantage that other reported absorbers do not have.

## 4 Conclusion

In this work, we introduce a novel concept for an ultra-wideband THz metasurface absorber free of metal components and utilizes carbon-based materials, namely graphite and graphene, in conjunction with a silica spacer and a graphite reflecting layer. In

comparison to conventional metal-based structures, this carbon metasurface absorber offers more consistent performance, tunable characteristics, enhanced absorption capabilities, and a more compact form factor. The absorption profiles of these carbon-based metasurface absorbers are intricately linked to the Fermi level of the graphene layer. By applying an adjustable voltage to the graphene layer to modify its Fermi level, the absorber's absorption bandwidth can be fine-tuned. At a Fermi level of 1 eV, the proposed absorber can achieve an impressively wide bandwidth of 8.99 THz, delivering over 90% absorption within the frequency range of 7.24–16.23 THz, with two distinct resonance peaks at 8.35 and 14.70 THz. Furthermore, thanks to the structural symmetry, this device exhibits insensitivity to changes in polarization angle. This research introduces an innovative design for a carbon-based ultra-wideband THz metasurface absorber, showcasing substantial potential applications in the fields of detection, imaging, and sensing especially in the biomedical field.

## Code and Data Availability

Data are available from authors upon reasonable request.

## Acknowledgments

This work was supported by the National Natural Science Foundation of China (Grant Nos. 62205204 and 62375172), the Natural Science Foundation of Shanghai (Grant No. 21ZR1446500), the Shanghai Local College Capacity Building Project (Grant No. 21010503200), and Shanghai

Normal University (Grant No. SK202240). The authors declare no conflicts of interest.

## References

- P. H. Siegel, "Terahertz technology," *IEEE Trans. Microwave Theory Tech.* **50**, 910–928 (2002).
- J. F. Federici et al., "THz imaging and sensing for security applications—explosives, weapons and drugs," *Semicond. Sci. Technol.* **20**, S266–S280 (2005).
- H.-J. Song and T. Nagatsuma, "Present and future of terahertz communications," *IEEE Trans. Terahertz Sci. Technol.* **1**, 256–263 (2011).
- H.-B. Liu et al., "Terahertz spectroscopy and imaging for defense and security applications," *Proc. IEEE* **95**, 1514–1527 (2007).
- C. Chen et al., "Terahertz metamaterial absorbers," *Adv. Mater. Technol.* **7**, 2101171 (2021).
- P. Gagnon et al., "Double-walled carbon nanotube film as the active electrode in an electro-optical modulator for the mid-infrared and terahertz regions," *J. Appl. Phys.* **128**, 233103 (2020).
- T. J. Cui et al., "Coding metamaterials, digital metamaterials and programmable metamaterials," *Light: Sci. Appl.* **3**, e218–e218 (2014).
- N. I. Zheludev and Y. S. Kivshar, "From metamaterials to meta-devices," *Nat. Mater.* **11**, 917–924 (2012).
- C. Xu et al., "Reconfigurable terahertz metamaterials: from fundamental principles to advanced 6G applications," *iScience* **25**, 103799 (2022).
- L. Qi and C. Li, "Multi-band terahertz filter with independence to polarization and insensitivity to incidence angles," *J. Infrared Millim. Terahertz Waves* **36**, 1137–1144 (2015).
- H. Tao et al., "A metamaterial absorber for the terahertz regime: Design, fabrication and characterization," *Opt. Express* **16**, 7181–7188 (2008).
- R. M. H. Bilal et al., "On the specially designed fractal metasurface-based dual-polarization converter in the THz regime," *Results Phys.* **19**, 103358 (2020).
- W. Cai et al., "Optical cloaking with metamaterials," *Nat. Photonics* **1**, 224–227 (2007).
- D. Ionescu and G. Apreotesei, "Metamaterial optical filter with maximal absorption coefficient," *MSE* **1182**, 012031 (2021).
- N. I. Landy et al., "Perfect metamaterial absorber," *Phys. Rev. Lett.* **100**, 207402 (2008).
- P. Yu et al., "Broadband metamaterial absorbers," *Adv. Opt. Mater.* **7**, 1800995 (2018).
- W. Li et al., "Metamaterial absorbers: from tunable surface to structural transformation," *Adv. Mater.* **34**, 2202509 (2022).
- B. Zhang and K.-D. Xu, "Switchable and tunable bifunctional THz metamaterial absorber," *J. Opt. Soc. Am. B* **39**, A52–A60 (2022).
- N. Hu et al., "Design of a multilayer broadband switchable absorber based on semiconductor switch," *IEEE Antennas Wirel. Propag. Lett.* **18**, 373–377 (2019).
- A. Beheshti Asl et al., "A perfect electrically tunable graphene-based metamaterial absorber," *J. Comput. Electron.* **20**, 864–872 (2021).
- X. Liu et al., "Ultra-wideband terahertz absorber based on metal-graphene hybrid structure," *Mater. Today Commun.* **34**, 105185 (2023).
- J. Lan et al., "Tunable broadband terahertz absorber based on laser-induced graphene," *Chin. Opt. Lett.* **20**, 073701 (2022).
- J. Yang et al., "Broadband terahertz absorber based on multi-band continuous plasmon resonances in geometrically gradient dielectric-loaded graphene plasmon structure," *Sci. Rep.* **8**, 3239 (2018).
- G. Wu et al., "Ultra-wideband tunable metamaterial perfect absorber based on vanadium dioxide," *Opt. Express* **29**, 2703–2711 (2021).
- Z. Liu et al., "A VO<sub>2</sub> film-based multifunctional metasurface in the terahertz band," *Chin. Opt. Lett.* **20**, 013602 (2022).
- H. Liu et al., "Vanadium dioxide-assisted broadband tunable terahertz metamaterial absorber," *Sci. Rep.* **9**, 5751 (2019).
- N. L. D. Grischkowsky, "Terahertz conductivity of thin metal films," *Appl. Phys. Lett.* **93**, 051105 (2008).
- M. Walther et al., "Terahertz conductivity of thin gold films at the metal-insulator percolation transition," *Phys. Rev. B* **76**, 125408 (2007).
- J. Lloyd-Hughes and T.-I. Jeon, "A review of the terahertz conductivity of bulk and nano-materials," *J. Infrared Millim. Terahertz Waves* **33**, 871–925 (2012).
- K. S. Novoselov et al., "A roadmap for graphene," *Nature* **490**, 192–200 (2012).
- A. Geim and K. Novoselov, "The rise of graphene," *Nat. Mater.* **6**, 183–191 (2007).
- F. Bonaccorso et al., "Graphene photonics and optoelectronics," *Nat. Photonics* **4**, 611–622 (2010).
- A. Andryieuski and A. V. Lavrinenko, "Graphene metamaterials based tunable terahertz absorber: effective surface conductivity approach," *Opt. Express* **21**(7), 9144–9155 (2013).
- L. Liu, A. Das, and C. M. Megaridis, "Terahertz shielding of carbon nanomaterials and their composites – a review and applications," *Carbon* **69**, 1–16 (2014).
- Q. Xing et al., "Tunable terahertz plasmons in graphite thin films," *Phys. Rev. Lett.* **126**, 147401 (2021).
- G. Varshney, "Wideband THz absorber: by merging the resonance of dielectric cavity and Graphite disk resonator," *IEEE Sens. J.* **21**, 1635–1643 (2021).
- G. Varshney, R. R. Gupta, and A. K. Sharma, "Near-perfect ultrabroadband metal-free ultrathin THz absorber," *J. Opt. Soc. Am. B* **40**, 21–27 (2022).
- A. K. Soni, P. Giri, and G. Varshney, "Metal-free super-wideband THz absorber for electromagnetic shielding," *Phys. Scr.* **96**, 125866 (2021).
- M. Rahmzadeh, H. Rajabalipanah, and A. Abdolali, "Multilayer graphene-based metasurfaces: robust design method for extremely broadband, wide-angle, and polarization-insensitive terahertz absorbers," *Appl. Opt.* **57**, 959–968 (2018).
- P. Zhang et al., "Ultra-broadband tunable terahertz metamaterial absorber based on double-layer vanadium dioxide square ring arrays," *Micromachines* **13**, 669 (2022).
- S. Zakir et al., "Polarization-insensitive, broadband, and tunable terahertz absorber using slotted-square graphene meta-rings," *IEEE Photonics J.* **15**, 1–8 (2023).
- P. Chamorro-Posada et al., "THz TDS study of several sp<sup>2</sup> carbon materials: graphite, needle coke and graphene oxides," *Carbon* **98**, 484–490 (2016).
- G. W. Hanson, "Dyadic green's functions for an anisotropic, non-local model of biased graphene," *IEEE Trans. Antennas Propag.* **56**, 747–757 (2008).
- J. S. Gómez-Díaz and J. Perruisseau-Carrier, "Graphene-based plasmonic switches at near infrared frequencies," *Opt. Express* **21**, 15490–15504 (2013).
- D. R. Smith et al., "Electromagnetic parameter retrieval from inhomogeneous metamaterials," *Phys. Rev. E* **71**, 036617 (2005).
- X. Chen et al., "Robust method to retrieve the constitutive effective parameters of metamaterials," *Phys. Rev. E* **70**, 016608 (2004).
- J. Huang et al., "Broadband terahertz absorber with a flexible, reconfigurable performance based on hybrid-patterned vanadium dioxide metasurfaces," *Opt. Express* **28**, 17832–17840 (2020).
- S. K. Ghosh et al., "Tunable graphene-based metasurface for polarization-independent broadband absorption in lower Mid-Infrared (MIR) range," *IEEE Trans. Electromagn. Compat.* **62**, 346–354 (2020).
- C. Liu, L. Qi, and X. Zhang, "Broadband graphene-based metamaterial absorbers," *AIP Adv.* **8**, 015301 (2018).

Biographies of the authors are not available.